Noise-Robust High-Fidelity Ultrasound Imaging with a Flexible Silicone-based Metalens

Jia-Jie He(何佳杰), Jun-Hao Jiang(江竣豪), Hai-Jun Luo(罗海军), Zhan Chen(陈霑)
Citation: Chin. Phys. B. 35,104304 (2026). DOI: 10.1088/1674-1056/aeac03 | CSTR: 32038.14.CPB.aeac03
http://cpb.iphy.ac.cn; http://iopscience.iop.org/cpb

What follows is a list of articles you may be interested in

Frequency–wavenumber migration for orthogonal plane wave imaging using row–column-addressed arrays

Jia Liu(刘佳), Chen Jiang(江晨), Chengcheng Liu(刘成成), Kailiang Xu(许凯亮), Dean Ta(他得安)
Chin. Phys. B. 35, 094302 (2026). DOI: 10.1088/1674-1056/ae1e67 | CSTR: 32038.14.CPB.ae1e67

Three-dimensional frequency-wavenumber method for efficient and high-quality volumetric ultrasound imaging

Huchang Guan(关虎昌), Chen Jiang(江晨), Kailiang Xu(许凯亮), Dean Ta(他得安)
Chin. Phys. B. 35, 074301 (2026). DOI: 10.1088/1674-1056/ae42b9 | CSTR: 32038.14.CPB.ae42b9

A tunable acoustic metasurface via one-dimensional mechanical adjustment for real-time focusing

Jie Hu(胡洁), Mengqi Jiang(姜梦琦), Rui Zang(藏瑞), Yuhang Qian(钱宇航)
Chin. Phys. B. 34, 104301 (2025). DOI: 10.1088/1674-1056/add7ac | CSTR: 32038.14.CPB.add7ac

Stabilized adaptive waveform inversion for enhanced robustness in Gaussian penalty matrix parameterization and transcranial ultrasound imaging

Jun-Jie Zhao(赵俊杰), Shan-Mu Jin(金山木), Yue-Kun Wang(王月坤), Yu Wang(王裕), Ya-Hui Peng(彭亚辉)
Chin. Phys. B. 34, 084301 (2025). DOI: 10.1088/1674-1056/add4f3 | CSTR: 32038.14.CPB.add4f3

Sobolev space norm regularized full waveform inversion for ultrasound computed tomography

Panpan Li(李盼盼), Yubing Li(李玉冰), Chang Su(苏畅), Zeyuan Dong(董则元), Weijun Lin(林伟军)
Chin. Phys. B. 34, 054301 (2025). DOI: 10.1088/1674-1056/adbbc0 | CSTR: 32038.14.CPB.adbbc0

Noise-robust high-fidelity ultrasound imaging with a flexible silicone-based metalens

Jia-Jie He(何佳杰)[†], Jun-Hao Jiang(江竣豪), Hai-Jun Luo(罗海军), and Zhan Chen(陈霑)[‡]

College of Electronic Information Engineering, Chongqing Normal University, Chongqing 401331, *China*

(Received 24 July 2026; revised manuscript received 10 September 2026; accepted manuscript online 24 September 2026)

Ultrasound imaging has been extensively employed in biomedical diagnosis and clinical research, owing to its compelling merits of non-ionizing radiation, cost-effectiveness, and real-time visualization. However, conventional ultrasound imaging systems are fundamentally constrained by diffraction-limited spatial resolution and insufficient conformability to complex biological tissue surfaces. Here, we design and fabricate a flexible Fresnel zone plate ultrasound metalens with transparent silicone-based materials, which is endowed with improved imaging resolution, excellent tissue conformability, and high acoustic-optical transmittance. Both experiments and simulations show that the proposed metalens achieves high-fidelity reconstruction of curved and linear contours from the letter-shaped "D/F" phantoms at 1 MHz. Further comparative imaging investigations on a customized "CQNU" pattern at 2 MHz demonstrate that the flexible metalens-based imaging method outperforms conventional plane-wave imaging in terms of ultrasound contrast and imaging quality. Additionally, the noise robustness of the metalens-based imaging system is evaluated by reconstructing a numeric target "702489" under varied input signal-to-noise ratios of 10 dB, 0 dB, and −10 dB. The well-resolved ultrasound images and quantitative imaging metrics manifest the remarkable noise tolerance and anti-interference capability of the metalens, enabling stable and high-quality imaging in complex, noisy biomedical scenarios. This flexible metalens-based imaging system holds great promise for advancing next-generation high-fidelity, conformal, and wearable ultrasound and photoacoustic bioimaging devices.

Keywords: acoustic metalens, ultrasound imaging, noise robustness

PACS: 43.30.+m, 43.35.+d

DOI: 10.1088/1674-1056/aeac03 **CSTR:** 32038.14.CPB.aeac03

1. Introduction

Ultrasound imaging plays an indispensable role in biomedical diagnosis, clinical screening, and wearable ultrasound devices.[1–5] Compared with conventional imaging modalities including x-ray, computed tomography (CT), and magnetic resonance imaging (MRI), ultrasound imaging offers distinct superiorities, such as non-ionizing radiation for safe diagnosis, real-time dynamic visualization, satisfactory deep-tissue penetration, and cost-effective operation.[6–11] Therefore, ultrasound imaging technology has been widely used in both clinical practice and daily healthcare scenarios, significantly facilitating practical biomedical examinations. Traditional ultrasound imaging technologies typically rely on piezoelectric wafer arrays, where acoustic focusing and imaging are realized through geometric lenses or electronic delay beamforming.[12,13] However, the lateral resolution of such systems is fundamentally constrained by the physical diffraction limit, thereby hindering subwavelength-scale imaging.[14,15] Furthermore, the rigid structure of traditional ultrasonic probes and array elements prevents flexible adaptation to complex biological tissue surfaces, which induces severe acoustic impedance mismatch and undesirable interface scattering.[16–18]

The rapid advancement of metasurfaces and metalenses[19–24] has effectively overcome the drawbacks of phased-array imaging techniques, offering a promising route toward high-performance subwavelength-resolution ultrasound imaging. Acoustic metalenses enable precise manipulation of acoustic wavefronts at the subwavelength scale.[25–30] Driven by the great progress of ultrasound imaging technologies, a variety of acoustic metalens architectures have been developed, including the negative-index,[31,32] space-coiling,[33–35] resonator-based,[36–38] super-oscillation[39,40] and phase-gradient modulation structures[41,42] types. Acoustic Fresnel zone plate (FZP) metalenses have also attracted intensive research interest, due to the ultrathin planar geometry, facile fabrication process, and superior imaging performance.[43–46] Moreover, the replacement of rigid structures with flexible silicone materials has significantly improved the practical applications of acoustic metalenses in biomedical scenarios.[47–49] The soft texture of silicone material enables tight conformal contact with complex biological surfaces, and the tissue-matched acoustic impedance effectively suppresses interfacial acoustic attenuation and scattering. In addition, high acoustic and optical transmittance of the transparent silicone-based metalens would resolve the spatial

[†]Corresponding author. E-mail: jiajiehe@cqnu.edu.cn

[‡]Corresponding author. E-mail: chenzhan@cqnu.edu.cn

© 2026 Chinese Physical Society and IOP Publishing Ltd. All rights, including for text and data mining, AI training, and similar technologies, are reserved.

coupling mismatch between acoustic and optical propagation paths in photoacoustic imaging, which facilitates the realization of coaxial and synergistic imaging. These advantages help to provide a feasible and promising technical foundation for the development of highly miniaturized, integrated, and multi-functional bioimaging devices.

In this work, we design and fabricate an FZP-based ultrasound metalens, and systematically validate its high-quality imaging performance and noise robustness capability. Numerical simulations and experimental measurements are carried out at 1 MHz with the letter-shaped targets "D/F", to characterize the imaging ability for both curved and linear features. The measured results show good agreement with simulations in terms of target morphology, contour details, and acoustic intensity distribution. No obvious shape distortions or imaging artifacts are observed, which demonstrates the high reliability and precision of the proposed metalens for ultrasound imaging. Furthermore, comparative simulations between the metalens-based imaging and plane-wave imaging are performed at 2 MHz with a customized "CQNU" pattern target, which confirms that the metalens enables a remarkable improvement in imaging contrast, clarity, and overall quality. In addition, noise robustness tests are conducted with a numeric target "702489" to evaluate the imaging stability under different noisy conditions. The metalens-based system reconstructs high-fidelity ultrasound images even at the input signal-to-noise ratios (input SNR) of 10 dB, 0 dB, and −10 dB, showing the superior anti-interference performance and strong environmental adaptability. This work verifies the noise-robust and high-fidelity imaging capability of the flexible metalens at different operating frequencies via quantitative metrics and side-by-side comparison with conventional plane-wave imaging, and expands its application prospects toward photoacoustic multimodal imaging and wearable real-time health monitoring.

2. Theory and design

Figure 1 schematically illustrates and compares the acoustic wave propagation behaviors of the metalens-based imaging and conventional plane-wave imaging. As depicted in Fig. 1(a), ultrasound metalens modulates the phase of incident plane waves and converges them into focused beams at the preset focal plane. After propagating through the target, the transmitted acoustic waves carrying abundant structural information are collected to realize high-fidelity image reconstruction. In contrast, conventional plane-wave imaging possesses no capability for active wavefront modulation, as illustrated in Fig. 1(b). Upon interaction with the target, incident ultrasound waves suffer substantial reflection, energy absorption, and severe wide-angle diffraction. These adverse effects ultimately result in blurred target contours and degraded contrast in the reconstructed images. The comparative analysis of working principles clearly reveals that the metalens-assisted focusing scheme effectively concentrates acoustic energy on the target plane and mitigates unwanted diffraction losses, establishing a fundamental prerequisite for achieving high-resolution ultrasound imaging.

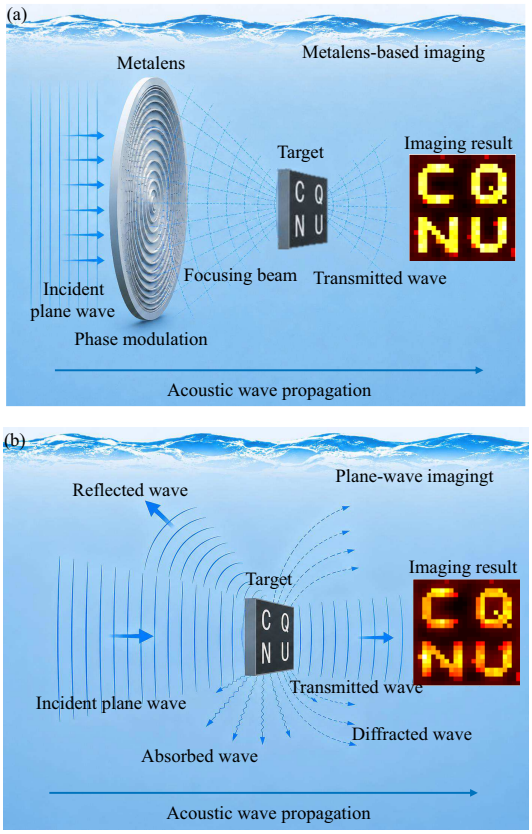

Fig. 1. Schematic comparison of acoustic wave propagation for ultrasound imaging. (a) The metalens-based imaging system conducts phase modulation on the incident plane waves to generate focused acoustic beams, enabling high-fidelity reconstruction of the target. (b) The conventional plane-wave imaging system suffers severe reflection, absorption and diffraction upon interaction with the target, leading to degraded imaging quality.

Figure 2 presents the structural design and fabrication route of the flexible metalens, as well as the corresponding ultrasound imaging experimental setup. Figure 2(a) displays the cross-sectional geometry of the designed FZP metalens, which is capable of precise phase modulation of incident ultrasound waves. Vertically incident plane waves with a wavelength of λ propagate through the metalens and converge at the predefined focal length F. The focused beams fully illuminate the imaging target, laying the basis for high-resolution ultrasound imaging. The metalens consists of concentric annular grooves with variable widths w_i and identical depth d, arranged on a substrate with thickness t. By adjusting the geometric dimensions of these annular grooves, a targeted π phase shift is introduced between adjacent zones, thereby converting incident planar wavefronts into converging spherical wavefronts. The radial width of each annular zone complies

with the theoretical FZP formula as $w_i = \sqrt{i\lambda F + (i\lambda/2)^2} - \sqrt{(i-1)\lambda F + [(i-1)\lambda/2]^2}$, and the groove depth satisfies $d = \lambda c/(2c_1)$,[50,51] where $c = 1500$ m/s and $c_1 = 980$ m/s denote the sound speed in water and silicone material, respectively.

The metalens is fabricated from flexible silicone material featuring high transmittance for both sound waves and visible light. The complete fabrication route is depicted in Fig. 2(b). First, a stereolithography (SLA) 3D printer is utilized to produce a concave female mold patterned with the concentric FZP ring structures. Then, silicone base and curing agent are mixed at a fixed proportion and thoroughly homogenized. The degassed mixture is poured into the mold to fully fill all annular grooves. After thermal curing in a thermostatic chamber, the integrated flexible silicone FZP metalens is carefully demolded. Figure 2(c) schematically shows the underwater imaging experimental platform, which consists of three core functional modules: ultrasound excitation, imaging measurement, and signal acquisition. A signal generator produces customized excitation waveforms, which are further amplified by a power amplifier to drive the ultrasound transducer. The emitted plane waves pass through the FZP metalens for phase modulation and are precisely focused at the desired position. The imaging target is mounted on the focal plane and moved by a motorized scanning stage for imaging measurement. A hydrophone is fixed at the focal point and acquires the transmitted acoustic signals, which are subsequently recorded by an oscilloscope and processed via computer programming for image reconstruction. This integrated experimental setup offers stable, repeatable measurements for subwavelength imaging and quantitative performance evaluation of the flexible metalens.

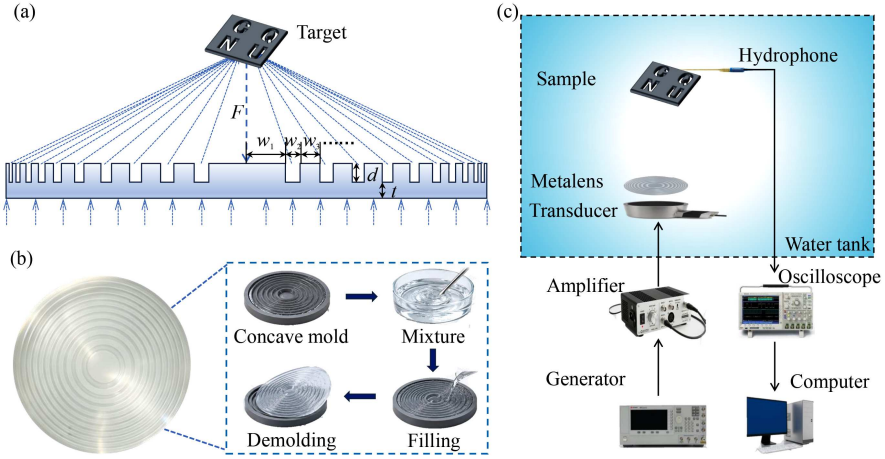

Fig. 2. Schematic diagram of the proposed FZP metalens and ultrasound imaging experimental setup. (a) Cross-sectional geometry of the flexible metalens. (b) Fabrication procedure of the silicone-based metalens. (c) Layout of the underwater ultrasound imaging experimental platform.

3. Results and discussion

In order to evaluate the ultrasound imaging performance of the designed metalens, we first perform imaging reconstruction utilizing the letter-shaped targets "D" and "F". Figure 3 presents the simulated and measured imaging results obtained at an operating frequency of 1 MHz. As displayed in Fig. 3(a), the original samples "D" and "F" are fabricated with a uniform line width of 2 mm, providing standard curved outlines and regular linear segments for qualitative imaging validation. The numerical simulations are performed using the Pressure Acoustics, Frequency Domain module in COMSOL Multiphysics, with three-dimensional models. The silicon-based metalens (sound speed: 980 m/s; density: 1050 kg/m^3) and imaging target (sound speed: 2400 m/s; density: 1200 kg/m^3) are fully immersed in water. Ultrasound waves at 1 MHz are vertically incident to the metalens, and converge at the focus spot by transmitting the metalens and target. The configurations of the imaging target are consistent with the experiment set-up. The reconstructed images are summarized in Figs. 3(b) and 3(c), showing excellent consistency between the simulations and experiments. It is evident that the proposed metalens enables high-fidelity reconstruction of both curved and linear target contours. The overall morphological profiles and fine structural details of the targets are clearly distinguished, without obvious shape distortion or severe imaging artifacts. These results demonstrate that the ultrasound metalens possesses a remarkable capability for reconstructing complex targets with hybrid curved and linear structures, which provides a reliable foundation for subsequent comparative imaging investigations.

To further validate the performance superiority of the metalens-based imaging method, comparative simulations are performed using a customized "CQNU" patterned target at 2 MHz. Figure 4(a) presents the original target with hollow "CQNU" letter features etched on a metallic substrate, which contains abundant intricate contours and narrow gaps of 1 mm. As shown in Fig. 4(b), the metalens-based imaging method accurately reconstructs nearly all subtle outlines and sharp edge

details of the target. In contrast, the conventional plane-wave imaging result in Fig. 4(c) suffers from severe image blurring and incomplete feature restoration. For quantitative evaluation, acoustic intensity profiles along the pink dashed lines marked in the images are extracted and plotted in Fig. 4(d). The intensity curve obtained from the metalens-based imaging method presents sharper peaks and deeper valleys, which contributes to significantly improved imaging contrast at the target geometric boundaries. By comparison, the plane-wave imaging curve shows weakened intensity responses and indistinct peak–valley transitions, demonstrating inferior resolution in capturing fine structural information. Figure 4(e) compares the intensity profiles extracted along the green dashed lines, where the plane-wave scheme yields an overall low acoustic intensity with trivial fluctuations, whereas the metalens-based imaging achieves prominently higher acoustic intensity and more pronounced peak–valley oscillations. These imaging results together with intensity analysis validate that the proposed ultrasound metalens delivers substantial improvements in imaging contrast, clarity, and spatial resolution over conventional plane-wave imaging.

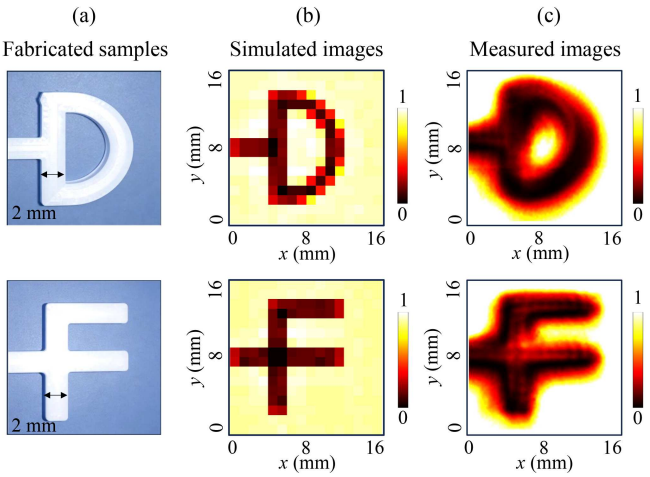

Fig. 3. Imaging reconstructions of the letter-shaped targets "D" and "F" in simulations and experiments at 1 MHz. (a) Photographs of the original fabricated samples. (b) Simulated ultrasound images. (c) Experimentally measured images.

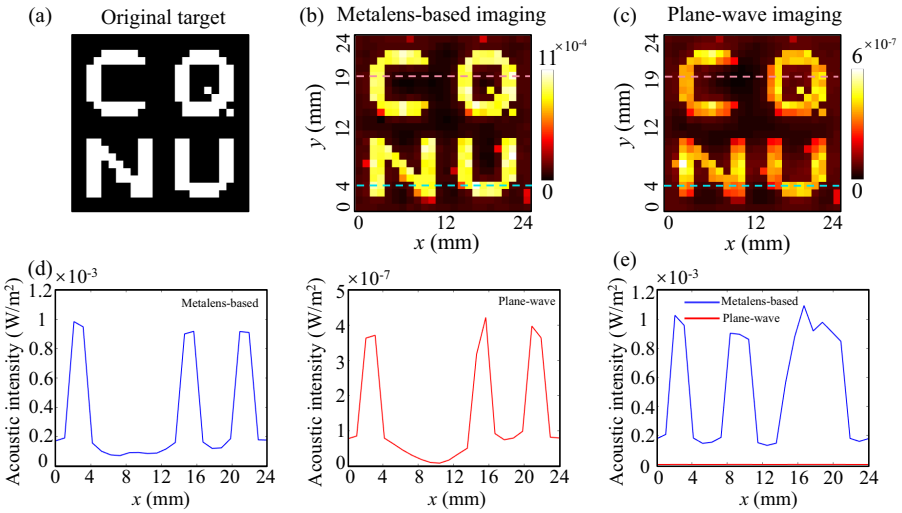

Fig. 4. Comparative imaging results of the "CQNU" pattern target at 2 MHz. (a) Original target with the smallest hollow gap of 1 mm. (b) Reconstructed image obtained via the metalens-based imaging method. (c) Reconstructed image from conventional plane-wave imaging method. (d) Extracted acoustic intensity profiles along the pink dashed lines in ultrasound images. (e) Comparison of acoustic intensity profiles along the green dashed lines.

Noise robustness simulations with additive Gaussian noise are performed to systematically evaluate the anti-interference performance of metalens-based imaging and conventional plane-wave imaging methods. Figures 5(a) and 5(b) present the noise-free imaging results of the numeric target "702489" acquired by the two imaging schemes at 2 MHz, respectively. Visually, the images reconstructed via the metalens-based strategy exhibit superior clarity and contrast relative to plane-wave imaging. Furthermore, Gaussian noise corresponding to input SNRs of 10 dB, 0 dB, and −10 dB is subsequently introduced into the imaging system to simulate noisy working environments. With the gradual increase of noise intensity, the metalens-based imaging scheme effectively suppresses noise artifacts and retains clear, distinguishable target contours under all noise conditions (Fig. 5(c)). In sharp contrast, the reconstructed images from conventional plane-wave imaging suffer drastic quality degradation in noisy environments. The fine target contours are severely obscured by background noise, and the structural features become progressively unrecognizable, accompanied by serious geometric distortion (Fig. 5(d)).

For quantitative assessment of imaging quality under noisy conditions, three universal image evaluation metrics are adopted, including root-mean-square error (RMS_{err}), output signal-to-noise ratio (output SNR), and structural similarity index (SSIM). The statistical results summarized in Fig. 5(e) reveal that the metalens-based imaging method (blue bars) achieves lower RMS_{err}, as well as higher output SNR and SSIM values than conventional plane-wave imaging (pink bars) under identical input noise conditions. When the in-

put noise rises from the noise-free state to an input SNR of −10 dB, RMS_{err} of the metalens-based imaging method decreases from 0.162 to 0.133, while that of plane-wave imaging increases from 0.207 to 0.417. Over the same noise variation range, output SNR of the metalens-based method rises from 9.604 to 11.318, whereas planewave imaging suffers a sharp drop from 7.499 to 1.403. Similarly, SSIM of the metalens-based imaging improves from 0.792 to 0.861, in contrast to a pronounced decrease for plane-wave imaging from 0.723 to 0.181. Higher output SNR and SSIM values represent more faithful retention of target geometric features, while reduced RMS_{err} reflects enhanced reconstruction precision, which quantitatively demonstrate a significant and stable improvement in ultrasound image quality. Overall, both qualitative imaging results and quantitative metric analyses comprehensively confirm the remarkable noise tolerance and robust anti-interference capability of the developed flexible metalens, highlighting its excellent environmental adaptability for practical and complex biomedical ultrasound imaging scenarios.

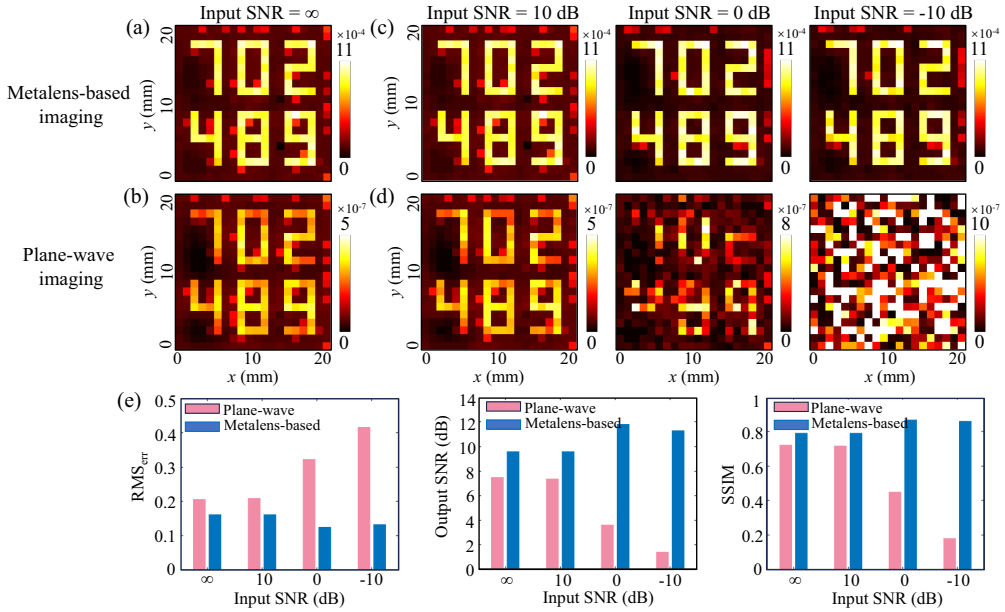

Fig. 5. Noise robustness comparison for imaging the numeric target "702489" under different input SNRs. (a) Noise-free image via metalens-based imaging method. (b) Noise-free image from plane-wave imaging. (c) Metalens-based imaging results under input SNRs of 10 dB, 0 dB and −10 dB. (d) Corresponding plane-wave images at the identical noise levels. (e) Quantitative comparison of RMS_{err}, output SNR and SSIM metrics from the images, confirming the strong environmental adaptability and reliable noise robustness of the metalens-based imaging system.

4. Conclusion

In summary, this work designs and fabricates an ultrasound FZP metalens based on flexible transparent silicone for high-performance biomedical imaging. The proposed metalens significantly improves the spatial resolution, and addresses insufficient conformability between rigid probes and biological tissue surfaces in traditional imaging systems. The letter-shaped "D/F" samples are imaged at 1 MHz ultrasound in experiments and simulations, demonstrating that the metalens exhibits superior high-fidelity capability in reconstructing both curved and linear target contours. Comparative simulations of complex "CQNU" pattern imaging further verify that the metalens-based strategy achieves substantial improvements in imaging clarity and contrast compared with conventional plane-wave imaging. Moreover, the anti-interference capability of the proposed metalens is verified by imaging a numeric target "702489" under different input SNR conditions (10 dB, 0 dB, and −10 dB). Quantitative evaluations reveal that the metalens-based imaging system yields lower RMS error, higher output SNR, and improved SSIM values under noisy environments, which highlights its strong noise robustness and environmental adaptability. This work would offer a promising and effective strategy for the development of ultrasound imaging devices, holding great potential for portable superficial ultrasound imaging, flexible endoscopes bioimaging, photoacoustic imaging integration, and wearable real-time health monitoring.

Acknowledgements

The work is supported by the National Natural Science Foundation of China (Grant No. 12504531), the Natural Science Foundation Project of Chongqing (Grant No. CSTB2025NSCQ-GPX1029), and the Chongqing Municipal Education Commission Science and Technology Project (Grant No. KJQN202500528).

References

[1] Chen S C, Ouyang Q L, Miao X B, Zhang F, Chen Z H, Qian X Y, Xie J W and Yan Z 2025 *Nano-Micro Lett.* **18** 45
[2] Huang C C, Chen P Y, Peng P H and Lee P Y 2017 *Med. Phys.* **44** 2185

[3] Pu C, Fu B, Lu P, Guan X, Zhang J, Shen Y, Li X, Guo L, Xu H, Jiang X and Peng C 2025 *Cell Rep. Phys. Sci.* **6** 102684
[4] Wang P X, Ma H Y, Liu T Y, Liu C C, Li D and Ta D A 2025 *Chin. Phys. B* **34** 044301
[5] Zhao J J, Jin S M, Wang Y K, Wang Y and Peng Y H 2025 *Chin. Phys. B* **34** 084301
[6] Zhang C X, Xiao H J, Jiang X and Ta D A 2026 *Adv. Sci.* **13** e75563
[7] Lin Z B, Liu J Z, Hu Y, Li Z L, Li P Q, Peng Y G, Li B and Zhu X F 2026 *Adv. Energy Mater.* **16** e06618
[8] Zhang Q D, Lin Z B, Chen Z, Liu Z H, He J L, Song J J, Zeng L S, Zhou L, Ding M Y, Peng Y G, Yuchi M and Zhu X F 2026 *Adv. Sci.* **13** e20560
[9] Chen J, Liu B, Peng G S, Zhou L M, Tan C G, Qin J L, Li J, Hong Z J, Wu Y J, Lu M H, Cai F Y and Huang Y H 2025 *Adv. Sci.* **12** 2500170
[10] Yin J, Huang L, Zhang J, Lok U W, DeRuiter R M, Zhu X, Krier J D, Kim Y, Zhao Y, Ji K, Lucien F, Lerman L O, Chen S and Huang C 2025 *BME Front.* **7** 0234
[11] Guan H C, Jiang C, Xu K L and Ta D A 2026 *Chin. Phys. B* **35** 074301
[12] Roberts M, Martin E, Brown M D, Cox B T and Treeby B E 2023 *IEEE Trans. Ultrason. Ferroelectr. Freq. Control* **70** 782
[13] Alasaarela E and Koivukangas J 1990 *J. Ultrasound Med.* **9** 23
[14] Chen R M, Jiang L M, Zhang T F, Matsuoka T, Yamazaki M, Qian X J, Lu G X, Safari A, Zhu J G, Shung K K, Ma T and Zhou Q F 2019 *IEEE Trans. Biomed. Eng.* **66** 1580
[15] Lin J and Ma C 2025 *Sci. Adv.* **11** eado2826
[16] Li Z X, Yang S H, Zhou M Q, Hou C X, Chen D D, Fei C L, Li D, Quan Y and Yang Y T 2024 *J. Adv. Dielectr.* **14** 2350001
[17] Yuan J W, Li Z K, Zhao Y H, *et al.* 2025 *Sci. Adv.* **11** eadw7632
[18] Xia Z, He H Z, Zhou Z X, Pan S S and Zhang S 2026 *Sensors* **26** 1992
[19] Zhu H 2025 *Natl. Sci. Rev.* **12** nwae366
[20] Liu D G, Hao L M, Zhu W R, Yang X, Yan X L, Guan C, Xie Y, Pang S F and Chen Z 2023 *Materials* **16** 7044
[21] Jin Y B, Kumar R, Poncelet O, Mondain-Monval O and Brunet T 2019 *Nat. Commun.* **10** 143
[22] Zhou Z L, Huang S B, Li D T, Zhu J and Li Y 2022 *Natl. Sci. Rev.* **9** nwab171
[23] Xie Y B, Wang W Q, Chen H Y, Konneker A, Popa B-I and Cummer S A 2014 *Nat. Commun.* **5** 5553
[24] Fan L J and Mei J 2023 *Phys. Rev. Appl.* **20** 054053
[25] Deng K, Ding Y Q, He Z J, Zhao H P, Shi J and Liu Z Y 2009 *J. Appl. Phys.* **105** 124909
[26] Liu T, Chen F, Liang S J, Gao H and Zhu J 2019 *Phys. Rev. Appl.* **11** 034061
[27] Ambati M, Fang N, Sun C and Zhang X 2007 *Phys. Rev. B* **75** 195447
[28] Chen J, Xiao J, Lisevych D, Shakouri A and Fan Z 2018 *Nat. Commun.* **9** 4920
[29] Sun H Y, Wang S, Huang S L, Peng L S, Wang Q and Zhao W 2020 *Sci. Rep.* **10** 1469
[30] Du X Y, Chen A L, Chong X Y, Zhao S D and Wang Y S 2024 *Int. J. Mech. Sci.* **264** 108851
[31] Lu M H, Zhang C, Feng L, Zhao J, Chen Y F, Mao Y W, Zi J, Zhu Y Y, Zhu S N and Ming N B 2007 *Nat. Mater.* **6** 744
[32] Liu F M and Liu Z Y 2015 *Phys. Rev. Lett.* **115** 175502
[33] Wang W Q, Xie Y B, Konneker A, Popa B I and Cummer S A 2014 *Appl. Phys. Lett.* **105** 101904
[34] Song G Y, Huang B, Dong H Y, Cheng Q and Cui T J 2016 *Sci. Rep.* **6** 35929
[35] Li Y, Liang B, Tao X, Zhu X F, Zou X Y and Cheng J C 2012 *Appl. Phys. Lett.* **101** 233508
[36] Li Y, Qi S B and Assouar M B 2016 *New J. Phys.* **18** 043024
[37] Tian Z H, Shen C, Li J F, Reit E, Gu Y Y, Fu H, Cummer S A and Huang T J 2019 *Adv. Funct. Mater.* **29** 1808489
[38] Zhu J, Zhu X F, Yin X B, Wang Y and Zhang X 2020 *Phys. Rev. Appl.* **13** 041001
[39] Shen Y X, Peng Y G, Cai F, Huang K, Zhao D G, Qiu C W, Zheng H and Zhu X F 2019 *Nat. Commun.* **10** 3411
[40] Fan L J and Mei J 2023 *Phys. Rev. Appl.* **19** 024026
[41] Guo J W, Qu R H, Fang Y, Yi W and Zhang X 2023 *Int. J. Mech. Sci.* **237** 107822
[42] Ju F F, Tian Y, Cheng Y and Liu X J 2018 *Appl. Phys. Lett.* **113** 121901
[43] Tarrazó-Serrano D, Pérez-López S, Candelas P, Uris A and Rubio C 2019 *Sci. Rep.* **9** 7067
[44] Jiménez N, Romero-García V, García-Raffi L M, Camarena F and Staliunas K 2018 *Appl. Phys. Lett.* **112** 204101
[45] Pan X, Zeng L S, Li Y, Zhu X F and Jin Y B 2023 *Ultrasonics* **128** 106876
[46] Calvo D C, Thangawng A L, Nicholas M and Layman C N 2015 *Appl. Phys. Lett.* **107** 014103
[47] He J J, Jiang X and Ta D A 2025 *Phys. Rev. Appl.* **23** 044039
[48] He J J, Jiang X, Zhang C X, Li Y, Liu C C, Liu X, Li B Y, Peng H S and Ta D A 2024 *Small* **20** 2312221
[49] Li M, Guo H Y, Su G Y, Liu Y Q and Lu T Q 2025 *Int. J. Mech. Sci.* **307** 110924
[50] Xia X X, Cai F Y, Li F, Meng L, Ma T, Zhou H, Ke M Z, Qiu C Y, Liu Z Y and Zheng H R 2019 *Adv. Mater. Technol.* **4** 1800542
[51] Xia X X, Li Y C, Cai F Y, Zhou H, Ma T and Zheng H R 2020 *Appl. Phys. Lett.* **117** 021904